

1      **High-level cognition is supported by at least second order**  
2      **dynamic correlations in neural activity patterns**

3      Lucy L. W. Owen<sup>1</sup>, Thomas H. Chang<sup>1,2</sup>, and Jeremy R. Manning<sup>1,†</sup>

<sup>1</sup>Department of Psychological and Brain Sciences,  
Dartmouth College, Hanover, NH

<sup>3</sup>Amazon.com, Seattle, WA

<sup>†</sup>Address correspondence to jeremy.r.manning@dartmouth.edu

4      August 8, 2019

5      **Abstract**

6      Our thoughts arise from coordinated patterns of interactions between brain structures that change  
7      with our ongoing experiences. High-order dynamic correlations in brain activity patterns reflect different  
8      subgraphs of the brain’s connectome that display homologous lower-level dynamic correlations. We tested  
9      the hypothesis that high-level cognition is supported by high-order dynamic correlations in brain activity  
10     patterns. We developed an approach to estimating high-order dynamic correlations in timeseries data,  
11     and we applied the approach to neuroimaging data collected as human participants either listened to a  
12     ten-minute story or a temporally scrambled version of the story, or underwent a resting state scan. We  
13     trained across-participants pattern classifiers to decode (in held-out data) when in the session each activity  
14     snapshot was collected. We found that classifiers trained to decode from high-order dynamic correlations  
15     yielded better performance on data collected as participants listened to the (unscrambled) story. By  
16     contrast, classifiers trained to decode data from scrambled versions of the story or during the resting  
17     state scan yielded the best performance when they were trained using first-order dynamic correlations  
18     or raw activity patterns. We suggest that as our thoughts become more complex, they are supported by  
19     higher-order patterns of dynamic network interactions throughout the brain.

20     **Introduction**

21     A central goal in cognitive neuroscience is to elucidate the *neural code*: the mapping between (a) mental  
22     states or cognitive representations and (b) neural activity patterns. One means of testing models of the  
23     neural code is to ask how accurately that model is able to “translate” neural activity patterns into known  
24     (or hypothesized) mental states or cognitive representations (e.g., ?????????). Training decoding models  
25     on different types of neural features can also help to elucidate which specific aspects of neural activity  
26     patterns are informative about cognition– and, by extension, which types of neural activity patterns might  
27     comprise the neural code. For example, prior work has used region of interest analyses to estimate the  
28     anatomical locations of specific neural representations (e.g., ?), or to compare the relative contributions to  
29     the neural code of multivariate activity patterns versus patterns of dynamic correlations between neural  
30     activity patterns (e.g., Fong et al., 2019; Manning et al., 2018). An emerging theme in this literature is that

<sup>31</sup> cognition is mediated by complex dynamic interactions between brain structures (Demertzi et al., 2019;  
<sup>32</sup> Turk-Browne, 2013; ?; ?).

<sup>33</sup> Studies of the neural code to date have primarily focused on univariate or multivariate neural pat-  
<sup>34</sup> terns (for review see , NormEtal06) or (more recently) on patterns of dynamic first-order correlations (i.e.,  
<sup>35</sup> interactions between pairs of brain structures; Fong et al., 2019; Manning et al., 2018). We wondered what  
<sup>36</sup> the future of this line of work might hold. For example, is the neural code mediated by higher-order  
<sup>37</sup> interactions between brain structures? Second-order correlations reflect *homologous* patterns of correlation.  
<sup>38</sup> In other words, if the changing patterns of correlations between two regions, *A* and *B*, are similar to those  
<sup>39</sup> between two other regions, *C* and *D*, this would be reflected in the second-order correlations between (*A*–*B*)  
<sup>40</sup> and (*C*–*D*). In this way, second-order correlations identify similarities and differences between subgraphs  
<sup>41</sup> of the brain’s connectome. Analogously, third-order correlations reflect homologies between second-order  
<sup>42</sup> correlations—i.e., homologous patterns of homologous interactions between brain regions. More generally,  
<sup>43</sup> higher-order correlations reflect homologies between patterns of lower-order correlations. We can then ask:  
<sup>44</sup> which “orders” of interaction are most reflective of high-level cognitive processes?

<sup>45</sup> Another central question pertains to the extent to which the neural code is carried by activity patterns that  
<sup>46</sup> directly reflect ongoing cognition (e.g., following ??), versus the dynamic properties of the network structure  
<sup>47</sup> itself, independent of specific activity patterns in any given set of regions (e.g., following ?). For example,  
<sup>48</sup> graph theoretic measures such as centrality and degree (?) may be used to estimate how a given brain  
<sup>49</sup> structure is “communicating” with other structures, independently of the specific neural representations  
<sup>50</sup> carried by those structures. If one considers a brain region’s graph theoretic position in the network (e.g.,  
<sup>51</sup> its eigenvector centrality) as a dynamic property, one can compare how the positions of different regions are  
<sup>52</sup> correlated, and/or how those patterns of correlations change over time. We can also compute higher-order  
<sup>53</sup> patterns in these correlations to characterize homologous subgraphs in the connectome that display similar  
<sup>54</sup> changes in their constituent brain structures’ interactions with the rest of the brain.

<sup>55</sup> To gain insights into the above aspects of the neural code, we developed a computational framework  
<sup>56</sup> for estimating dynamic high-order correlations in timeseries data. This framework provides an important  
<sup>57</sup> advance, in that it enables us to examine patterns in higher-order correlations that are computationally  
<sup>58</sup> intractable to estimate via conventional methods. Given a multivariate timeseries, our framework pro-  
<sup>59</sup> vides timepoint-by-timepoint estimates of the first-order correlations, second-order correlations, and so  
<sup>60</sup> on (up to tenth-order correlations in this manuscript). Our approach combines a kernel-based method  
<sup>61</sup> for computing dynamic correlations in timeseries data with a dimensionality reduction step that projects  
<sup>62</sup> the resulting dynamic correlations into a low-dimensional space. We explored two dimensionality reduc-  
<sup>63</sup> tion approaches: principle components analysis (PCA; Pearson, 1901), which preserves an approximately

64 invertible transformation back to the original data; and a second non-invertible algorithm that explored  
65 patterns in eigenvector centrality (?). This latter approach characterizes correlations between each feature  
66 dimension's relative *position* in the network in favor of the specific activity histories of different features.

67 We validated our approach using synthetic data where the underlying correlations were known. We  
68 then applied our framework to a neuroimaging dataset collected as 125 participants listened to either an  
69 audio recording of a ten-minute story or a temporally scrambled version of the story, or underwent a resting  
70 state scan (Simony et al., 2016). We used a subset of the data to train across-participant classifiers to decode  
71 listening times using a blend of neural features (comprising neural activity patterns, as well as different  
72 orders of correlations between those patterns that were inferred using our computational framework).  
73 We found that both the PCA-based and eigenvector centrality-based approaches yielded neural patterns  
74 that could be used to decode accurately. Both approaches also yielded the best decoding accuracy for  
75 data collected during (intact) story listening when high-order (PCA: second-order; eigenvector centrality:  
76 fourth-order) dynamic correlation patterns were included as features. When we trained classifiers on the  
77 scrambled stories or resting state data, only lower-order dynamic patterns were informative to the decoders.  
78 Taken together, our results indicate that high-level cognition is supported by high-order dynamic patterns  
79 of communication between brain structures. **JRM STOPPED HERE**

## 80 Methods

81 A major challenge to studying such patterns is that typically neither the correlations nor the hierarchical  
82 organizations of those correlations may be directly observed. Rather, these fundamental properties must  
83 be inferred indirectly by examining the observable parts of the system—e.g., the behaviors of the individual  
84 units of that system. Here we propose a series of mathematical operations that may be used to approximate  
85 dynamic correlations at a range of scales (i.e., orders of interaction).

86 There are two basic steps to our approach (Fig. 2). In the first step, we take a number-of-timepoints ( $T$ )  
87 by number-of-features ( $F$ ) *matrix of observations* ( $\mathbf{X}$ ) and we return a  $T$  by  $\frac{F^2-F}{2}$  *matrix of dynamic correlations*  
88 ( $\mathbf{Y}$ ). Here  $\mathbf{Y}_0$  describes, at each moment, how all of the features (columns of  $\mathbf{X}$ ) are inferred to be interacting.  
89 (Since the interactions are assumed to be non-recurrent and symmetric, only the upper triangle of the full  
90 correlation matrix is computed.) In the second step, we project  $\mathbf{Y}_0$  onto an  $F$ -dimensional space, resulting in  
91 a new  $T$  by  $F$  matrix  $\mathbf{Y}_1$ . Note that  $\mathbf{Y}_1$  contains information about the correlation dynamics present in  $\mathbf{X}$ , but  
92 represented in a compressed number of dimensions. By repeatedly applying these two steps in sequence,  
93 we can examine and explore higher order dynamic correlations in  $\mathbf{X}$ .

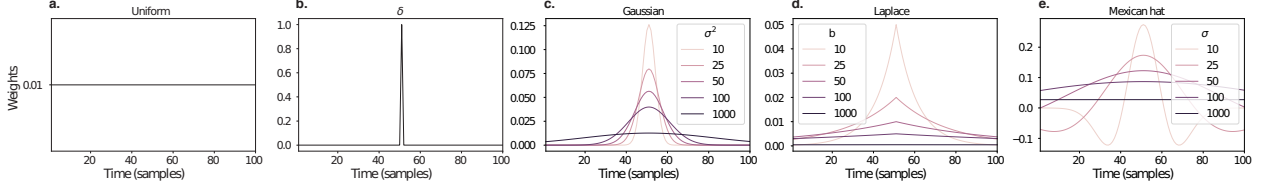


Figure 1: **Examples of time-varying weights.** Each panel displays per-timepoint weights at  $t = 50$ , evaluated for 100 timepoints (1, ..., 100). **a. Uniform weights.** The weights are timepoint-invariant; observations at all timepoints are weighted equally, and do not change as a function of  $t$ . This is a special case of weight function that reduces dynamic correlations to static correlations. **b. Dirac delta function.** Only the observation at timepoint  $t$  is given weight (of 1), and weights for observations at all other timepoints are set to 0. **c. Gaussian weights.** Each observation's weights fall off in time according to a Gaussian probability density function centered on  $\mu = t$ . Weights derived using several different example variance parameters ( $\sigma^2$ ) are displayed. **d. Laplace weights.** Each observation's weights fall off in time according to a Laplace probability density function centered on  $\mu = t$ . Weights derived using several different example scale parameters ( $b$ ) are displayed. **e. Mexican hat (Ricker wavelet) weights.** Each observation's weights fall off in time according to a Ricker wavelet centered on  $t$ . This function highlights the *contrasts* between local versus surrounding activity patterns in estimating dynamic correlations. Weights derived using several different example width parameters ( $\sigma$ ) are displayed.

## 94 Dynamic correlations

Given a matrix of observations, we can compute the (static) correlations between any pair of observations,  $\mathbf{X}_i$  and  $\mathbf{X}_j$  using:

$$\text{corr}(\mathbf{X}_i, \mathbf{X}_j) = \frac{\sum_{t=1}^T (\mathbf{X}_i(t) - \bar{\mathbf{X}}_i)(\mathbf{X}_j(t) - \bar{\mathbf{X}}_j)}{\sqrt{\sum_{t=1}^T \sigma_{\mathbf{X}_i}^2 \sigma_{\mathbf{X}_j}^2}}, \text{ where} \quad (1)$$

$$\bar{\mathbf{X}}_k = \sum_{t=1}^T \mathbf{X}_k(t), \text{ and} \quad (2)$$

$$\sigma_{\mathbf{X}_k}^2 = \sum_{t=1}^T (\mathbf{X}_k(t) - \bar{\mathbf{X}}_k)^2 \quad (3)$$

95     We can generalize this formula to compute time-varying correlations by incorporating a *weight function*  
96     that takes a time  $t$  as input, and returns how much the observed data every timepoint (including  $t$ ) contribute  
97     to the correlations at time  $t$  (Fig. 1).

Given a weight function  $w(t)$  for timepoint  $t$ , evaluated at timepoints in the interval  $[1, \dots, T]$ , we can

extend the static correlation formula in Equation 2 to reflect an *instantaneous correlation* at timepoint  $t$ :

$$\text{timecorr}(\mathbf{X}_i, \mathbf{X}_j, t) = \frac{\sum_{t=1}^T (\mathbf{X}_i(t) - \tilde{\mathbf{X}}_i(t))(\mathbf{X}_j(t) - \tilde{\mathbf{X}}_j(t))}{\sqrt{\sum_{t=1}^T \tilde{\sigma}_{\mathbf{X}_i}^2(t) \tilde{\sigma}_{\mathbf{X}_j}^2(t)}}, \text{ where} \quad (4)$$

$$\tilde{\mathbf{X}}_k(t) = \sum_{i=1}^T w(t, i) \mathbf{X}_k(i), \quad (5)$$

$$\tilde{\sigma}_{\mathbf{X}_k}^2(t) = \sum_{i=1}^T (\mathbf{X}_k(i) - \tilde{\mathbf{X}}_k(t))^2, \quad (6)$$

and  $w(t, i)$  is shorthand for  $w(t)$  evaluated at timepoint  $i$ . Equation 5 may be used to estimate the instantaneous correlations between every pair of observations, at each timepoint (i.e.,  $\mathbf{Y}$ ).

#### 100 Inter-subject dynamic correlations

Equation 5 provides a means of taking a single observation matrix,  $\mathbf{X}$  and estimating the dynamic correlations from moment to moment,  $\mathbf{Y}$ . Suppose that one has access to a set of multiple observation matrices that reflect the same phenomenon. For example, one might collect neuroimaging data from several experimental participants, as each participant performs the same task (or sequence of tasks). Let  $\mathbf{X}_1, \mathbf{X}_2, \dots, \mathbf{X}_P$  reflect the  $T$  by  $F$  observation matrices for each of  $P$  participants in an experiment. We can use *inter-subject functional connectivity* (ISFC; Simony et al., 2016) to compute the degree of stimulus-driven correlations reflected in the multi-participant dataset at a given timepoint  $t$  using:

$$\bar{\mathbf{C}}(t) = M \left( R \left( \frac{1}{2P} \sum_{i=1}^P Z(Y_i(t))^T + Z(Y_i(t)) \right) \right), \quad (7)$$

where  $M$  extracts and vectorizes the diagonal and upper triangle of a symmetric matrix,  $Z$  is the Fisher z-transformation (Zar, 2010):

$$Z(r) = \frac{\log(1+r) - \log(1-r)}{2} \quad (8)$$

$R$  is the inverse of  $Z$ :

$$R(z) = \frac{\exp(2z-1)}{\exp(2z+1)}, \quad (9)$$

and  $\mathbf{Y}_i(t)$  denotes the correlation matrix (Eqn. 2) between each column of  $\mathbf{X}_i$  and each column of the average observations from all *other* participants,  $\bar{\mathbf{X}}_{\setminus i}$ :

$$\bar{\mathbf{X}}_{\setminus i} = R \left( \frac{1}{P-1} \sum_{i \in \setminus i} Z(\mathbf{X}_i) \right), \quad (10)$$

101 where  $\setminus i$  denotes the set of all participants other than participant  $i$ . In this way, the  $T$  by  $\left(\frac{F^2-F}{2} + F\right)$  matrix  $\bar{\mathbf{C}}$   
102 is the time-varying extension of the ISFC approach developed by Simony et al. (2016).

### 103 Higher-order correlations

104 Given a timeseries of dynamic correlations (e.g., obtained using Eqn. 5), higher-order correlations reflect the  
105 dynamic correlations between columns of  $\mathbf{Y}$ . Given unlimited computing resources, one could use repeated  
106 applications of Equation 5 to estimate these higher-order correlations (i.e., substituting in the previous  
107 output,  $\mathbf{Y}$ , for the input,  $\mathbf{X}$  in the equation). However, because each output  $\mathbf{Y}$  has  $O(F^2)$  columns relative  
108 to  $F$  columns in the input  $\mathbf{X}$ , the output of Equation 5 grows with the square of the number of repeated  
109 applications (total cost of computing  $n^{\text{th}}$  order correlations is  $O(F^{2n})$  for  $n \in \mathcal{J}, n > 0$ ). When  $F$  or  $n$  is large,  
110 this approach quickly becomes intractable.

111 To make progress in computing  $\mathbf{Y}_{n+1}$ , we can approximate  $\mathbf{Y}_n$  by computing an  $O(F)$ -dimensional em-  
112 bedding of  $\mathbf{Y}_n$ , termed  $\hat{\mathbf{Y}}_n$ , and then we can apply Equation 5 to  $\hat{\mathbf{Y}}_n$  rather than directly to  $\mathbf{Y}_n$ . This enables  
113 us to maintain  $O(n)$  scaling with respect to  $n$ , rather than exponential scaling via the direct approach.

114 There are many possible methods for computing  $\hat{\mathbf{Y}}_n$  from  $\mathbf{Y}_n$ , including traditional dimensionality  
115 reduction approaches and graph theory based approaches as described next. In the *Discussion* section we  
116 elaborate on other potential approaches.

### 117 Dimensionality reduction-based approaches to computing $\hat{\mathbf{Y}}_n$

118 Commonly used dimensionality reduction algorithms include Principal Components Analysis (PCA; Pear-  
119 son, 1901), Probabilistic PCA (PPCA; Tipping & Bishop, 1999), Exploratory Factor Analysis (EFA; Spearman,  
120 1904), Independent Components Analysis (ICA; Comon et al., 1991; Jutten & Herault, 1991), *t*-Stochastic  
121 Neighbor Embedding (*t*-SNE; van der Maaten & Hinton, 2008), Uniform Manifold Approximation and  
122 Projection (UMAP; McInnes & Healy, 2018), non-negative matrix factorization (NMF; Lee & Seung,  
123 1999), Topographic Factor Analysis (TFA) Manning et al. (2014), Hierarchical Topographic Factor analysis  
124 (HTFA) Manning et al. (2018), Topographic Latent Source Analysis (TLSA) Gershman et al. (2011), Dictio-  
125 nary learning (J. Mairal et al., 2009; J. B. Mairal et al., 2009), deep autoencoders (Hinton & Salakhutdinov,

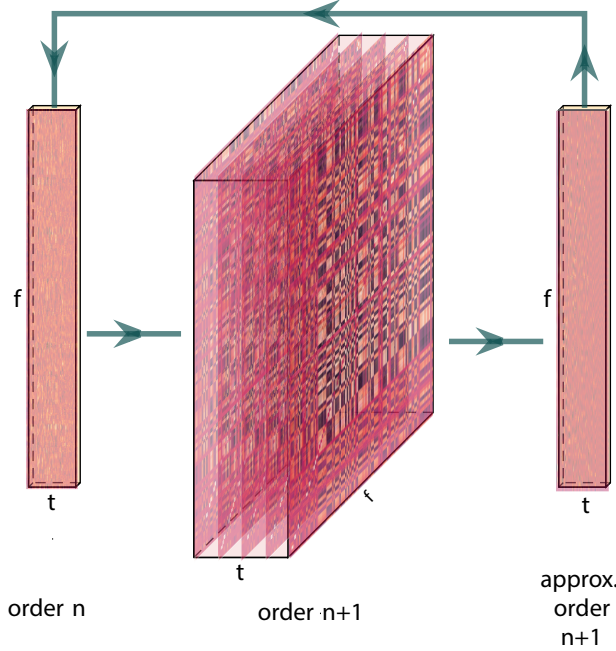


**Figure 2: Computing higher order correlations.** Dynamic correlations are computed then approximated to the same size as original data using dimensionality reduction. This process is repeated, and can be used to compute up to any arbitrary order with computations scaling linearly (as opposed to exponentially) with order.

126 2006), among others. While complete characterizations of each of these algorithms is beyond the scope of  
 127 the present manuscript, the general intuition driving these approaches is to compute the  $\hat{\mathbf{Y}}$  with  $i$  columns  
 128 that is closest to the original  $\mathbf{Y}$  with  $j$  columns, and where (typically)  $i \ll j$ . The different approaches place  
 129 different constraints on what properties  $\hat{\mathbf{Y}}$  must satisfy and which aspects of the data are compared (and  
 130 how) to characterize the match between  $\hat{\mathbf{Y}}$  and  $\mathbf{Y}$ .

131 Applying dimensionality reduction algorithms to  $\mathbf{Y}$  yields a  $\hat{\mathbf{Y}}$  whose columns reflect weighted combi-  
 132 nations (or nonlinear transformations) of the original columns of  $\mathbf{Y}$ . This has two main consequences. First,  
 133 with each repeated dimensionality reduction, the resulting  $\hat{\mathbf{Y}}_n$  has lower and lower fidelity (with respect to  
 134 what the “true”  $\mathbf{Y}_n$  might have looked like without using dimensionality reduction to maintain scalability).  
 135 In other words, computing  $\hat{\mathbf{Y}}_n$  is a lossy operation. Second, whereas the columns of  $\mathbf{Y}_n$  may be mapped  
 136 directly onto pairs of columns of  $\mathbf{Y}_{n-1}$ , that mapping either becomes less cleanly defined in  $\hat{\mathbf{Y}}_n$  due to the  
 137 reweightings and/or nonlinear transformations.

138 **Graph theory-based approaches to computing  $\hat{\mathbf{Y}}_n$**

139 Graph theoretic measures take as input a matrix of interactions (e.g., using the above notation, an  $F \times F$   
 140 correlation matrix or binarized correlation matrix reconstituted from a single timepoint’s row of  $\mathbf{Y}$ ) and

141 return as output a set of  $F$  measures describing how each node (feature) sits within that interactions matrix  
142 with respect to the rest of the population. Common measures include betweenness centrality (the proportion  
143 of shortest paths between each pair of nodes in the population that involves the given node in question; e.g.,  
144 Barthélemy, 2004; Freeman, 1977; Geisberger et al., 2008; Newman, 2005; Opsahl et al., 2010); diversity and  
145 dissimilarity (characterizations of how differently connected a given node is from others in the population;  
146 e.g., Lin, 2009; Rao, 1982; Ricotta & Szeidl, 2006); Eigenvector centrality and pagerank centrality (measures of  
147 how influential a given node is within the broader network; e.g., Bonacich, 2007; Halu et al., 2013; Lohmann  
148 et al., 2010; Newman, 2008); transfer entropy and flow coefficients (a measure of how much information is  
149 flowing from a given node to other nodes in the network; e.g., Honey et al., 2007; Schreiber, 2000);  $k$ -coreness  
150 centrality (a measure of the connectivity of a node within its local sub-graph; e.g., Alvarez-Hamelin et al.,  
151 2005; Christakis & Fowler, 2010); within-module degree (a measure of how many connections a node has to  
152 its close neighbors in the network; e.g., Rubinov & Sporns, 2010); participation coefficient (a measure of the  
153 diversity of a node's connections to different sub-graphs in the network; e.g., Rubinov & Sporns, 2010); and  
154 sub-graph centrality (a measure of a node's participation in all of the network's sub-graphs; e.g., Estrada &  
155 Rodríguez-Velázquez, 2005).

156 As an alternative to the above dimensionality reduction approach to embedding  $\mathbf{Y}_n$  in a lower-dimensional  
157 space, but still allowing for scalable explorations of higher-order structure in the data, we also explore using  
158 the above graph theoretic measures as a means of obtaining  $\hat{\mathbf{Y}}_n$ . In particular: for a given graph theoretic  
159 measure,  $\eta : \mathcal{R}^{F \times F} \rightarrow \mathcal{R}^F$ , we can use  $\eta$  to transform each row of  $\mathbf{Y}_n$  in a way that characterizes the cor-  
160 responding graph-theoretic properties of each column. Whereas the dimensionality reduction approach  
161 to computing  $\hat{\mathbf{Y}}_n$  is lossy, the graph-theory approach is lossless. However, whereas the dimensionality  
162 reduction approach maintains ties (direct or indirect) to the original activity patterns reflected in  $\mathbf{Y}_{n-1}$ , the  
163 graph-theory approach does not. Instead, the graph-theory characterizes the nature and timecourse of each  
164 feature's *participation* in the network.

## 165 Evaluation metrics

166 We evaluate our approach to extracting dynamic correlations and higher-order correlations using several  
167 metrics detailed next. First, we generated synthetic data using known time-varying correlations, and then  
168 we evaluated the fidelity with which Equation 5 could recover those correlations (for synthetic datasets  
169 with different properties, and using different kernels to define the weights; Fig. 1). We then turned to a  
170 series of analyses on a (real) neuroimaging dataset where the ground truth correlations were *not* known.  
171 We evaluated whether the recovered correlations could be used to accurately label held-out neuroimaging

172 data with the time at which it was collected. We used this latter evaluations (using timepoint decoding)  
173 as a proxy for gauging how much explanatory power the recovered correlations held with respect to the  
174 observed data.

175 **Generating synthetic data**

176 To explore recovery of a constant covariance (Fig. 3, a.), we generated synthetic data sampled from a constant  
177 covariance matrix. To do this, we created one random covariance matrix,  $K$ , with 50 features, and for each  
178 of the 300 timepoints we sampled from a Gaussian distribution centered on  $K$ . Similarly, we generated  
179 synthetic data sampled from a random covariance matrix (Fig. 3, b.) by creating a new random covariance  
180 matrix  $K(t)$ , for each of the 300 timepoints and sampled from a Gaussian distribution centered on  $K(t)$ .

To generate synthetic data from a dynamically changing covariance matrix (Fig. 3, c.), we generated two random covariance matrices,  $K_1$  and  $K_2$ . We then computed a weighted average covariance matrix for each of the 300 timepoint,  $K(t)$ , by taking the linearly spaced weights ( $w$ ) of the two random matrices,

$$K(t) = w(t) * K_1 + (1 - w(t)) * K_2, \quad (11)$$

$$(12)$$

181 and for each of the 300 timepoints sampled from a Gaussian distribution centered on  $K(t)$ .

182 Lastly, for the synthetic data containing block structure (Fig. 3, d.), we followed the same process of  
183 creating synthetic data sampled from a constant covariance matrix (see above) but sampled from a new  
184 random covariance matrix after 60 consecutive timepoints. We then pieced the blocks together to create a  
185 sythetic dataset with 300 total timepoints but drawn from 5 separate covariance matrices.

186 **Recovery of ground truth parameters from synthetic data**

187 We applied timecorr, using delta and gaussian (width = 10) kernels Fig. 1 to each of these synthetic datasets,  
188 then correlated each recovered correlation matrix with the ground truth. We repeated this process 10 times  
189 and explored how recovery varies with the kernel and the specific structure of the data. For the ramping  
190 synthetic dataset (Fig. 3, c.) and for the block synthetic dataset (Fig. 3, d.) we made further comparisons  
191 of the timecorr recovered correlation matrices. We compared the ramping recovered correlation matrices to  
192 only the first random covariance matrix  $K_1$  (First, Fig. 3, c.) and to only the last random covariance matrix  
193  $K_2$  (Last, Fig. 3, c.) from Equation 12. We also compared the block recovered correlation matrices in to the  
194 block specific covariance matrix (Block 1-5, Fig. 3, d.).

195 **Timepoint decoding**

196 To explore how higher-order structure varies with stimulus structure and complexity, we used a previous  
197 neuroimaging dataset Simony et al. (2016) in which participants listened to an audio recording of a story;  
198 36 participants listen to an intact version of the story, 17 participants listen to time-scrambled recordings of  
199 the same story where paragraphs were scrambled, 36 participants listen to word-scrambled version and 36  
200 participants lay in rest condition.

201 Prior work has shown participants share similar neural responses to richly structured stimuli when  
202 compared to stimuli with less structure. To assess whether the moment-by-moment higher order correlations  
203 were reliably preserved across participants, we used inter-subject functional connectivity (ISFC) to isolate  
204 the time-varying correlational structure (functional connectivity patterns that were specifically driven by  
205 the story participants listened to. Following the analyses conducted by (HTFA) Manning et al. (2018), we  
206 first applied *hierarchical topographic factor analysis* (HTFA) to the fMRI datasets to obtain a time series of  
207 700 node activities for every participant. We then computed the dynamic weighted ISFC using a range of  
208 kernels and widths. Specifically, we used Gaussian, Laplace, and mexican hat kernels, as well as widths of  
209 5, 10, 20, and 50. We then approximated these dynamic correlation using two reduction measures, PCA and  
210 eigenvector centrality, and computed the dynamic weighted ISFC on the approximations. We repeated this  
211 process up to 10th order approximated correlations.

212 To assess decoding accuracy, we randomly divided participants for each stimulus into training and  
213 testing groups. For the zeroth order, we computed the mean factor activity for each group. For all subsequent  
214 orders up to the tenth order, we computed the mean approximated dynamic ISFC of factor activity for each  
215 group. To assess how additional higher-order correlations contribute to decoding accuracy, for each order  
216 we included a weighted-mixture (described below) of the activity patterns of all previous orders. For each  
217 group of participants in turn, we compared these activity patterns (using Pearson correlations) to estimate  
218 the story times each pattern corresponded to. Specifically, we asked, for each timepoint: what are the  
219 correlations between the first group's and second group's activity patterns at each order. We note that the  
220 decoding test we used is a conservative in which we count a timepoint label as incorrect if it is not an exact  
221 match.

222 For each order we obtained the weighted-mixture of the correlation matrices for the current order and  
223 all previous orders using mixing parameter,  $\phi$ , where  $0 < \phi < 1$  reflects a weighted mixture of order based  
224 decoding Fig. 4 Panel c. ). We calculated  $\phi$ , by subdividing the training group and using the quasi-Newton  
225 method of Broyden, Fletcher, Goldfarb, and Shanno (BFGS (Nocedal & Wright, 2006)) for optimization. We  
226 repeated this cross-validation process 10 times for each parameter set.

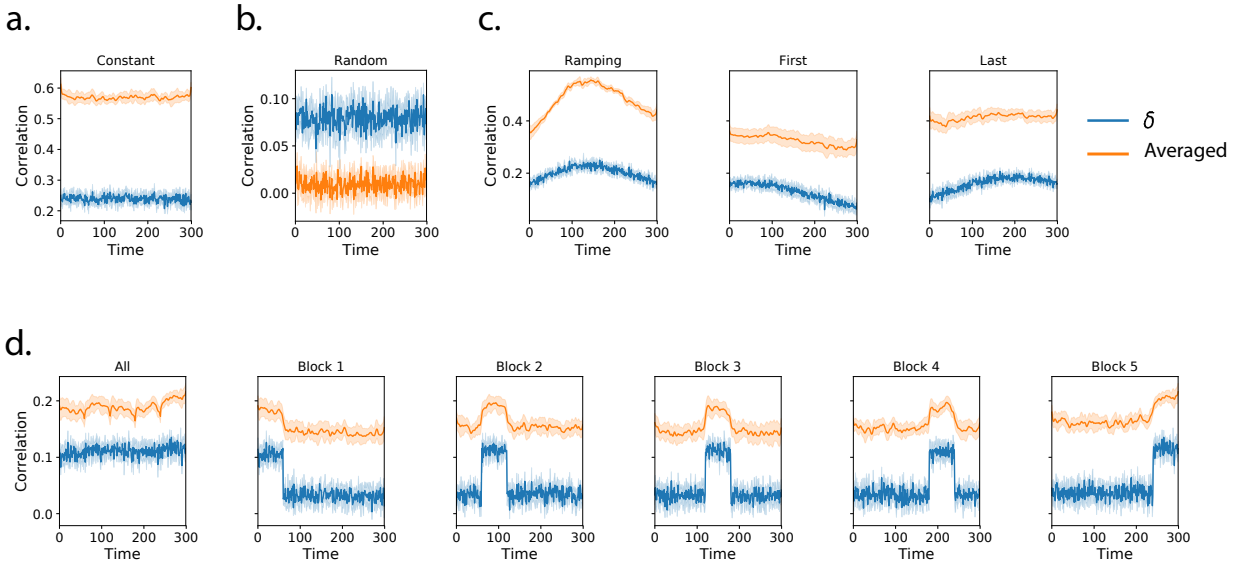


**Figure 3: Dynamic correlation recovery with synthetic data.** Using synthetic data containing different underlying correlational structure, we test how well we can recover dynamic correlation matrices using different kernels when compared to ground truth. We compare the results using a delta kernel with averaged results from several kernels (Gaussian, Laplace, and mexican hat) and several widths (5, 10, 20, and 50). We plot recovery using of datasets containing the following underlying structure: **a. Constant.** **b. Random.** **c. Ramping.** **d. Block.**

## 227 Results

### 228 Synthetic data

229 To assess the performance of dynamic correlation recovery using `timecorr`, we varied width the kernel and  
 230 the specific structure of the data. We applied `timecorr`, using delta and gaussian kernels Fig. 1) to each of  
 231 the following synthetic datasets: constant, random, ramping, and block. We then correlated each recovered  
 232 correlation matrix with the ground truth.

233 For the constant synthetic dataset, a gaussian kernel (width=10) outperformed the delta kernel (Fig. 3,  
 234 a.). This is in contrast with the random synthetic dataset, for which the delta kernel best captures the rapidly  
 235 changing structure (Fig. 3, b.). For the ramping synthetic dataset, the slow changing strucutre within the  
 236 data is best captured by the gaussian kernel and the best recovery occurs in the middle (Ramping, Fig. 3,  
 237 c.). In addition to comparing the `timecorr` recovered correlation matrices to the ground truth, we further  
 238 compared the ramping recovered correlation matrices to only the first random covariance matrix  $K_1$  (First,  
 239 Fig. 3, c.) and to only the last random covariance matrix  $K_2$  (Last, Fig. 3, c.), both of which perform best at  
 240 the beginning and end respectively.

241 Similary for the block sythetic dataset, we compared the `timecorr` recovered correlation matrices to

242 the ground truth as well as to each block-specific covariance matrix (Block 1-5, Fig. 3, d.). Although the  
243 structure is changing by block, the gaussian kernel once again outperforms the delta kernel. Performance  
244 does however drop near even boundaries for when using the gaussian kernel.

245 **Neuroimaging dataset (Simony et al., 2016)**

246 For our decoding analysis, we used HTFA-derived node activities Manning et al. (2018) from fMRI data  
247 collected as participants listened to an audio recording of a story (intact condition; 36 participants), lis-  
248 tened to time scrambled recordings of the same story (17 participants in the paragraph-scrambled condition  
249 listened to the paragraphs in a randomized order and 36 in the word-scrambled condition listened to  
250 the words in a randomized order), or lay resting with their eyes open in the scanner (rest condition; 36  
251 participants). We sought to demonstrate how higher-order correlations may be used to examine dynamic  
252 interactions of brain patterns in (real) multi-subject fMRI datasets. This story listening dataset was col-  
253 lected as part of a separate study, where the full imaging parameters, image preprocessing methods, and  
254 experimental details may be found (Simony et al., 2016). The dataset is available at [http://arks.prince-  
255 ton.edu/ark:/88435/dsp015d86p269k](http://arks.princeton.edu/ark:/88435/dsp015d86p269k).

256 We next evaluated if our model of high-order correlations in brain activity can capture cognitively  
257 relevant brain patterns. We performed a decoding analysis, using cross validation to estimate (using other  
258 participants' data) which parts of the story each weighted-mixture of higher-order brain activity pattern  
259 corresponded to (see *Materials and methods*). We note that our primary goal was not to achieve perfect  
260 decoding accuracy, but rather to use decoding accuracy as a benchmark for assessing whether different  
261 neural features specifically capture cognitively relevant brain patterns.

262 Separately for each experimental condition, we divided participants into two groups. For the zeroth  
263 order, we computed the mean factor activity for each group. For all subsequent orders up to the tenth  
264 order, we computed the mean approximated dynamic ISFC of factor activity for each group (see *Materials*  
265 and *methods*), and combined in a weighted mixutre with all previous orders (i.e. cross-validation for the  
266 second order contained a weighted-mixture of zeroth, first, and second order (Fig. 4, c.&f.). For each  
267 order, we correlated the group 1 activity patterns with group 2 activity patterns. We then subdivided  
268 the group 1 to obtain an optimal weighting parameter for each order's correlation matrix using the same  
269 cross validation method. We used the optimal weighting parameters to obtain a weighted-mixture (see  
270 *Materials and methods*) of each order's correlation matrix. Using these correlations, we labeled the group 1  
271 timepoints using the group 2 timepoints with which they were most highly correlated; we then computed  
272 the proportion of correctly labeled group 1 timepoints. (We also performed the symmetric analysis whereby

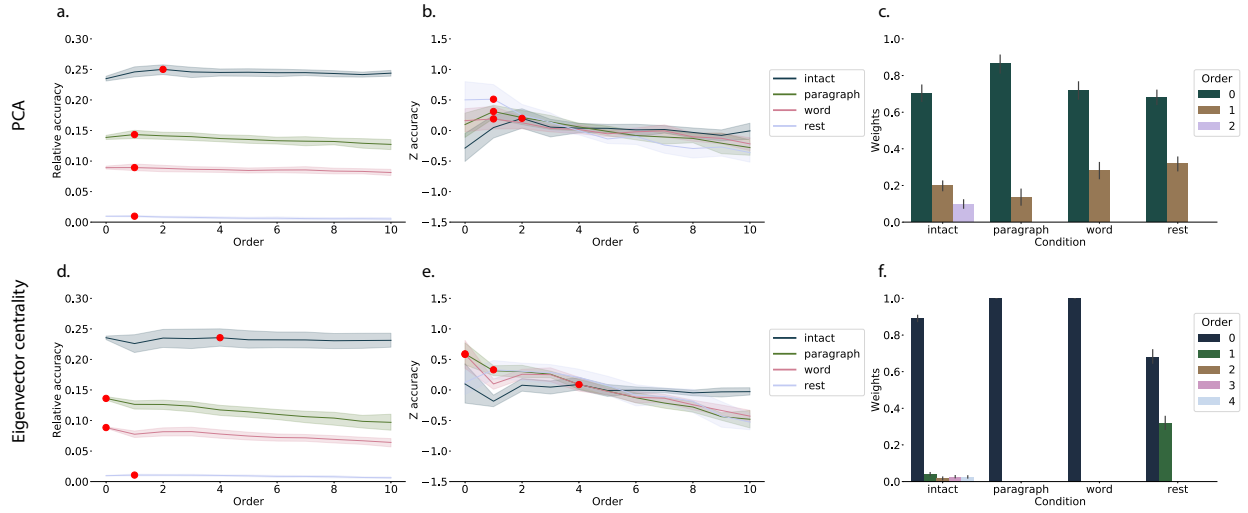


**Figure 4: Decoding by order.** **a.&d. Relative decoding accuracy by order.** Ribbons of each color display cross-validated decoding performance averaged over all parameters for each condition (intact, paragraph, word, and rest) using PCA (a.) or eigenvector centrality (d.) to approximate correlations. Decoders were trained using increasingly more higher-order information and this ribbons are displayed relative to chance at 0. The red dots indicates maximum decoding accuracy for each condition. **b.&e. Z-transformed decoding accuracy by order.** We Z-transformed the decoding accuracy by order to better visualize the order with the maximum decoding accuracy for each condition using PCA (b.) or eigenvector centrality (e.) to approximate correlations. **c.&f. Optimized weights.** Bar heights indicate the optimized mixing parameter  $\phi$  of each contributing order up to and including the order with the maximum decoding accuracy for each contributing order using PCA (c.) or eigenvector centrality (f.) to approximate correlations. For the order with maximum decoding accuracy by condition, we show barplots of the optimized weights  $\phi$  for each contributing order.

273 we labeled the group 2 timepoints using the group 1 timepoints as a template.) We repeated this procedure  
274 100 times (randomly re-assigning participants to the two groups each time) to obtain a distribution of  
275 decoding accuracies for each experimental condition. There were 272 timepoints for paragraph condition,  
276 300 timepoints for intact and word conditions, and 400 timepoints for rest condition, so chance performance  
277 on this decoding test is was  $\frac{1}{272}$ ,  $\frac{1}{300}$ , and  $\frac{1}{400}$  respectively.

278 We repeated this process for each set of parameters, varying kernel type and width, and averaged over the  
279 reduction technique used to approximate the higher-order correlations (PCA Fig. 4, a.-c. and eigenvector  
280 centrality Fig. 4, d.-f.). Since there is no ground truth in these analyses, and we did not know which  
281 parameters best capture the data, we instead report a robustness search by averaging over the parameters  
282 and reporting which results consistently showed up across all parameters.

283 The two methods used to approximate the higher-order correlations (PCA Fig. 4, a.-c. and eigenvector  
284 centrality Fig. 4, d.-f.) capture different facets of the activity patterns. Using PCA, the higher-order  
285 correlations are all linked to the original activity patterns, whereas eigenvector centrality breaks the  
286 immediate link with specific brain areas and instead characterizes the position of the nodes in the network  
287 that are similar over time.

288 We found for both PCA and eigenvector centrality, during the intact condition in the experiment,  
289 classifiers that incorporated higher-order correlations yielded consistently higher accuracy than classifiers  
290 trained only on lower-order patterns (Fig. 4, a.&d.). We plot the average correlations for up to the fourth  
291 order for the intact condition (Fig. 5) representing the degree of agreement by location pair over time. By  
292 contrast, we found that incorporating higher-order (greater than first order) correlations did not further  
293 improve decoding accuracy for the other listening conditions or rest condition. This suggests that the  
294 cognitive processing that supported the most cognitively rich condition involved higher-order network  
295 dynamics.

## 296 Discussion

297 Based on prior work (Demertzis et al., 2019) and following the direction of the field (Turk-Browne, 2013)  
298 we think our thoughts might be encoded in dynamic network patterns, and possibly higher order network  
299 patterns (Fig. 6). We sought to test this hypothesis by developing an approach to inferring high-order  
300 network dynamics from timeseries data.

301 One challenge in studying dynamic interactions is the computational resources required to calculate  
302 higher-order correlations. We developed a computationally tractable model of network dynamics (Fig. 2)  
303 that takes in a feature timeseries and outputs approximated first-order dynamics (i.e., dynamic functional

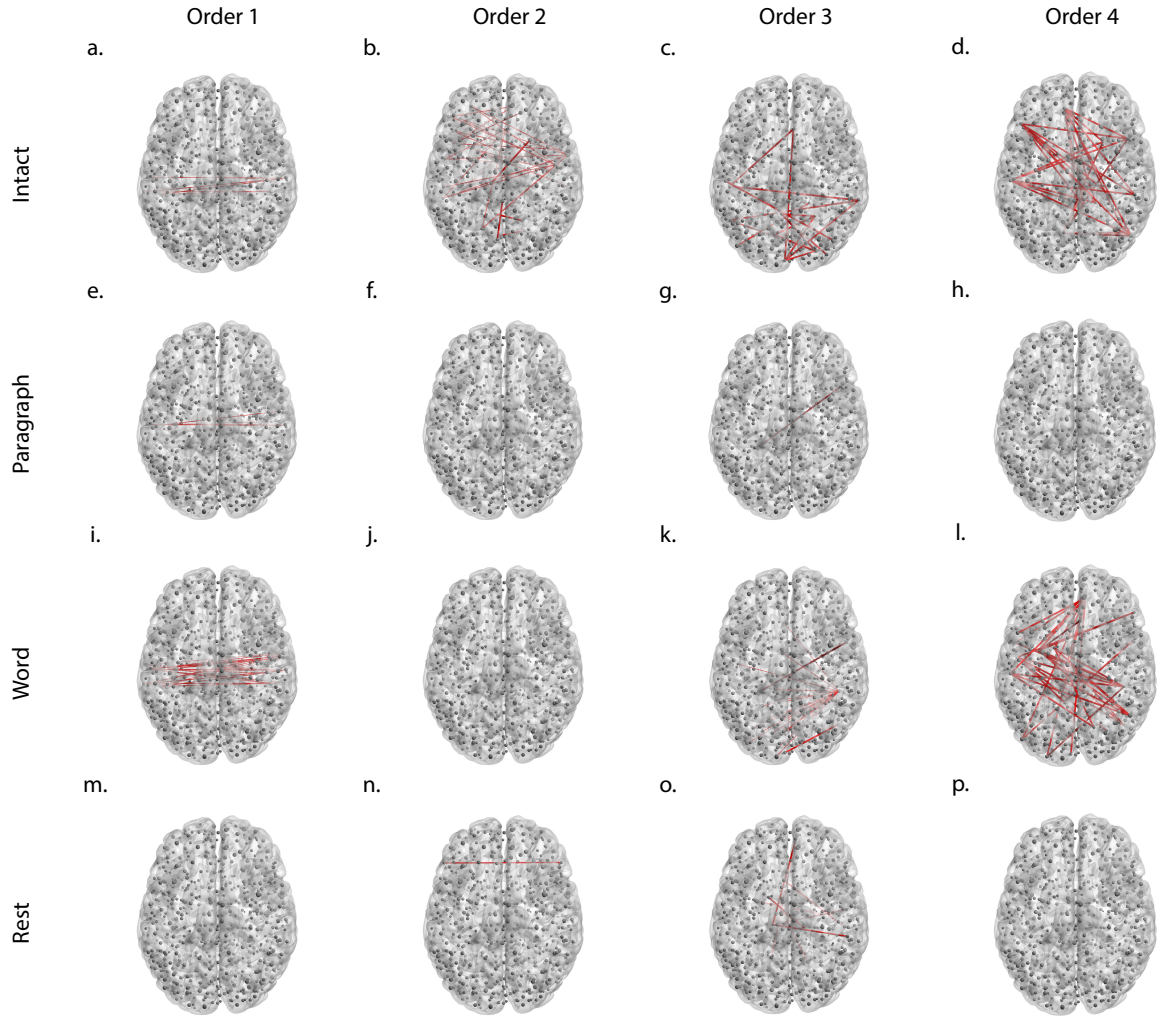


**Figure 5: Average correlations by order for the intact listening condition.** Using eigenvector centrality to approximate higher-order correlations for **a.-d.** intact, **e.-h.** paragraph scrambled, **i.-l.** word scrambled, and **m.-p.** rest conditions, we plot the strongest 25% absolute value mean correlation for first through fourth orders, representing the degree of agreement by location pair over time.

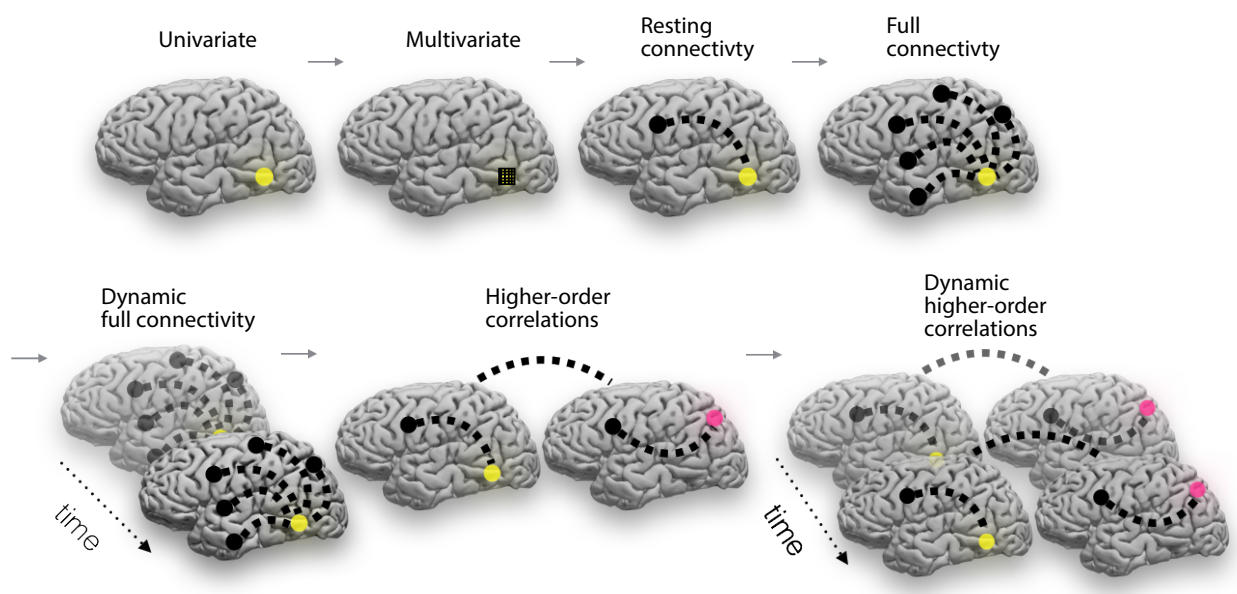


**Figure 6: Direction of the field (adapted from (Turk-Browne, 2013)).** The evolution of fMRI analyses started with univariate activation, which refers to the average amplitude of BOLD activity evoked by events of an experimental condition. Next, multivariate classifiers are trained on patterns of activation across voxels to decode distributed representations for specific events. The next, resting connectivity, is the temporal correlation of one or more seed regions with the remainder of the brain during rest. Additionally, task-based connectivity examines how these correlations differ by cognitive state. Following this increasing trajectory of increasing complexity, full connectivity considers all pairwise correlations in the brain, most commonly at rest. Next, dynamic full connectivity considers how full connectivity changes over time. Continuing this line of reasoning, we expect higher-order network dynamics might provide even richer insights into the neural basis of cognition.

304 correlations), second-order dynamics (reflecting homologous networks that dynamically form and disperse),  
305 and higher-order network dynamics (up to tenth-order dynamic correlations).

306 We first validated our model using synthetic data, and explored how recovery varied with different  
307 underlying data structures and kernels. We then applied the approach to an fMRI dataset (Simony et al.,  
308 2016) in which participants listened to an audio recording of a story, as well as scrambled versions of the  
309 same story (where the scrambling was applied at different temporal scales). We trained classifiers to take  
310 the output of the model and decode the timepoint in the story (or scrambled story) that the participants  
311 were listening to. We found that, during the intact listening condition in the experiment, classifiers that  
312 incorporated higher-order correlations yielded consistently higher accuracy than classifiers trained only  
313 on lower-order patterns (Fig. 4, a.&d.). By contrast, these higher-order correlations were not necessary  
314 to support decoding the other listening conditions and (minimally above chance) during a control rest  
315 condition. This suggests that the cognitive processing that supported the most cognitively rich listening  
316 conditions involved second-order (or higher) network dynamics.

317 Although we found decoding accuracy was best when incorporating higher-order network dynamics  
318 for all but rest condition, it is unclear if this is a product of the brain or the data collection technique. It could  
319 be that the brain is second-order or it could be that fMRI can only reliably give second-order interactions.  
320 Exploring this method with other data collection technique will be important to disentangle this question.

## 321 **Concluding remarks**

322 How can we better understand how brain patterns change over time? How can we quantify the potential  
323 network dynamics that might be driving these changes? One way to judge the techniques of the future is  
324 to look at the trajectory of the fMRI field so far has taken so far (Fig. 2). The field started with univariate  
325 activation, measuring the average activity for each voxel. Analyses of multivariate activation followed,  
326 looking at spatial patterns of activity over voxels. Next, correlations of activity were explored, first with  
327 measures like resting connectivity that take temporal correlation between a seed voxel and all other voxels  
328 then with full connectivity that measure all pairwise correlations. Additionally, this path of increasing  
329 complexity also moved from static to dynamic measurements. One logical next step in this trajectory would  
330 be dynamic higher-order correlations. We have created a method to support these calculations by scalably  
331 approximating dynamic higher-order correlations.

<sup>332</sup> **Acknowledgements**

<sup>333</sup> We acknowledge discussions with Luke Chang, Hany Farid, Paxton Fitzpatrick, Andrew Heusser, Eshin  
<sup>334</sup> Jolly, Qiang Liu, Matthijs van der Meer, Judith Mildner, Gina Notaro, Stephen Satterthwaite, Emily Whitaker,  
<sup>335</sup> Weizhen Xie, and Kirsten Ziman. Our work was supported in part by NSF EPSCoR Award Number 1632738  
<sup>336</sup> to J.R.M. and by a sub-award of DARPA RAM Cooperative Agreement N66001-14-2-4-032 to J.R.M. The  
<sup>337</sup> content is solely the responsibility of the authors and does not necessarily represent the official views of our  
<sup>338</sup> supporting organizations.

<sup>339</sup> **Author contributions**

<sup>340</sup> Concept: J.R.M. Implementation: T.H.C., L.L.W.O., and J.R.M. Analyses: L.L.W.O and J.R.M.

<sup>341</sup> **References**

- <sup>342</sup> Alvarez-Hamelin, I., Dall'Asta, L., Barrat, A., & Vespignani, A. (2005). *k*-corr decomposition: a tool for the  
<sup>343</sup> visualization of large scale networks. *arXiv*, cs/0504107v2.
- <sup>344</sup> Barthélemy, M. (2004). Betweenness centrality in large complex networks. *European Physical Journal B*, 38,  
<sup>345</sup> 163–168.
- <sup>346</sup> Bassett, D., Meyer-Lindenberg, A., Achard, S., Duke, T., & Bullmore, E. (2006, December). Adaptive  
<sup>347</sup> reconfiguration of fractal small-world human brain functional networks. *Proceedings of the National  
Academy of Sciences, USA*, 103(51), 19518-23.
- <sup>349</sup> Bonacich, P. (2007). Some unique properties of eigenvector centrality. *Social Networks*, 29(4), 555–564.
- <sup>350</sup> Bullmore, E., & Sporns, O. (2009). Complex brain networks: graph theoretical analysis of structural and  
<sup>351</sup> functional systems. *Nature Reviews Neuroscience*, 10(3), 186–198.
- <sup>352</sup> Christakis, N. A., & Fowler, J. H. (2010). Social network sensors for early detection of contagious outbreaks.  
<sup>353</sup> *PLoS One*, 5(9), e12948.
- <sup>354</sup> Comon, P., Jutten, C., & Herault, J. (1991). Blind separation of sources, part II: Problems statement. *Signal  
Processing*, 24(1), 11 - 20.

- 356 Demertzi, A., Tagliazucchi, E., Dehaene, S., Deco, G., Barttfeld, P., Raimondo, F., ... Sitt, J. D. (2019). Human  
357 consciousness is supported by dynamic complex patterns of brain signal coordination. *Science Advances*,  
358 5(2), eaat7603.
- 359 Estrada, E., & Rodríguez-Velázquez, J. A. (2005). Subgraph centrality in complex networks. *Physical Review*  
360 *E*, 71(5), 056103.
- 361 Etzel, J. A., Gazzola, V., & Keysers, C. (2009). An introduction to anatomical ROI-based fMRI classification.  
362 *Brain Research*, 1282, 114–125.
- 363 Fong, A. H. C., Yoo, K., Rosenberg, M. D., Zhang, S., Li, C.-S. R., Scheinost, D., ... Chun, M. M. (2019).  
364 Dynamic functional connectivity during task performance and rest predicts individual differences in  
365 attention across studies. *NeuroImage*, 188, 14–25.
- 366 Freeman, L. C. (1977). A set of measures of centrality based on betweenness. *Sociometry*, 40(1), 35–41.
- 367 Geisberger, R., Sanders, P., & Schultes, D. (2008). Better approximation of betweenness centrality. *Proceedings*  
368 *of the meeting on Algorithm Engineering and Experiments*, 90–100.
- 369 Gershman, S., Blei, D., Pereira, F., & Norman, K. (2011). A topographic latent source model for fMRI data.  
370 *NeuroImage*, 57, 89–100.
- 371 Halu, A., Mondragón, R. J., Panzarasa, P., & Bianconi, G. (2013). Multiplex PageRank. *PLoS One*, 8(10),  
372 e78293.
- 373 Haxby, J. V., Gobbini, M. I., Furey, M. L., Ishai, A., Schouten, J. L., & Pietrini, P. (2001). Distributed and  
374 overlapping representations of faces and objects in ventral temporal cortex. *Science*, 293, 2425–2430.
- 375 Hinton, G. E., & Salakhutdinov, R. R. (2006). Reducing the dimensionality of data with neural networks.  
376 *Science*, 313(5786), 504–507.
- 377 Honey, C. J., Kötter, R., Breakspear, M., & Sporns, O. (2007). Network structure of cerebral cortex shapes  
378 functional connectivity on multiple time scales. *Proceedings of the National Academy of Science USA*, 104(24),  
379 10240–10245.
- 380 Huth, A. G., de Heer, W. A., Griffiths, T. L., Theunissen, F. E., & Gallant, J. L. (2016). Natural speech reveals  
381 the semantic maps that tile human cerebral cortex. *Nature*, 532, 453–458.
- 382 Huth, A. G., Nisimoto, S., Vu, A. T., & Gallant, J. L. (2012). A continuous semantic space describes  
383 the representation of thousands of object and action categories across the human brain. *Neuron*, 76(6),  
384 1210–1224.

- 385 Jutten, C., & Herault, J. (1991). Blind separation of sources, part I: An adaptive algorithm based on  
386 neuromimetic architecture. *Signal Processing*, 24(1), 1–10.
- 387 Kamitani, Y., & Tong, F. (2005). Decoding the visual and subjective contents of the human brain. *Nature*  
388 *Neuroscience*, 8, 679–685.
- 389 Landau, E. (1895). Zur relativen Wertbemessung der Turnierresultate. *Deutsches Wochenschach*, 11, 366–369.
- 390 Lee, D. D., & Seung, H. S. (1999). Learning the parts of objects by non-negative matrix factorization. *Nature*,  
391 401, 788–791.
- 392 Lin, J. (2009). Divergence measures based on the Shannon entropy. *IEEE Transactions on Information Theory*,  
393 37(1), 145–151.
- 394 Lohmann, G., Margulies, D. S., Horstmann, A., Pleger, B., Lepsién, J., Goldhahn, D., … Turner, R. (2010).  
395 Eigenvector centrality mapping for analyzing connectivity patterns in fMRI data of the human brain.  
396 *PLoS One*, 5(4), e10232.
- 397 Mairal, J., Ponce, J., Sapiro, G., Zisserman, A., & Bach, F. R. (2009). Supervised dictionary learning. *Advances*  
398 *in Neural Information Processing Systems*, 1033–1040.
- 399 Mairal, J. B., Bach, F., Ponce, J., & Sapiro, G. (2009). Online dictionary learning for sparse coding. *Proceedings*  
400 *of the 26th annual international conference on machine learning*, 689–696.
- 401 Manning, J. R., Ranganath, R., Norman, K. A., & Blei, D. M. (2014). Topographic factor analysis: a Bayesian  
402 model for inferring brain networks from neural data. *PLoS One*, 9(5), e94914.
- 403 Manning, J. R., Zhu, X., Willke, T. L., Ranganath, R., Stachenfeld, K., Hasson, U., … Norman, K. A. (2018).  
404 A probabilistic approach to discovering dynamic full-brain functional connectivity patterns. *NeuroImage*,  
405 180, 243–252.
- 406 McInnes, L., & Healy, J. (2018). t-SNE: Uniform manifold approximation and projection for dimension  
407 reduction. *arXiv*, 1802(03426).
- 408 Mitchell, T., Shinkareva, S., Carlson, A., Chang, K., Malave, V., Mason, R., & Just, M. (2008). Predicting  
409 human brain activity associated with the meanings of nouns. *Science*, 320(5880), 1191.
- 410 Newman, M. E. J. (2005). A measure of betweenness centrality based on random walks. *Social Networks*, 27,  
411 39–54.
- 412 Newman, M. E. J. (2008). The mathematics of networks. *The New Palgrave Encyclopedia of Economics*, 2, 1–12.

- 413 Nishimoto, S., Vu, A., Naselaris, T., Benjamini, Y., Yu, B., & Gallant, J. (2011). Reconstructing visual  
414 experience from brain activity evoked by natural movies. *Current Biology*, 21, 1 - 6.
- 415 Nocedal, J., & Wright, S. J. (2006). *Numerical optimization*. New York: Springer.
- 416 Norman, K. A., Newman, E., Detre, G., & Polyn, S. M. (2006). How inhibitory oscillations can train neural  
417 networks and punish competitors. *Neural Computation*, 18, 1577–1610.
- 418 Opsahl, T., Agneessens, F., & Skvoretz, J. (2010). Node centrality in weighted networks: generalizing degree  
419 and shortest paths. *Social Networks*, 32, 245–251.
- 420 Pearson, K. (1901). On lines and planes of closest fit to systems of points in space. *The London, Edinburgh,  
421 and Dublin Philosophical Magazine and Journal of Science*, 2, 559-572.
- 422 Pereira, F., Lou, B., Pritchett, B., Ritter, S., Gershman, S. J., Kanwisher, N., . . . Fedorenko, E. (2018). Toward  
423 a universal decoder of linguistic meaning from brain activation. *Nature Communications*, 9(963), 1–13.
- 424 Rao, C. R. (1982). Diversity and dissimilarity coefficients: a unified approach. *Theoretical Population Biology*,  
425 21(1), 24–43.
- 426 Ricotta, C., & Szeidl, L. (2006). Towards a unifying approach to diversity measures: Bridging the gap  
427 between the Shannon entropy and Rao's quadratic index. *Theoretical Population Biology*, 70(3), 237–243.
- 428 Rubinov, M., & Sporns, O. (2010). Complex network measures of brain connectivity: uses and interpreta-  
429 tions. *NeuroImage*, 52, 1059–1069.
- 430 Schreiber, T. (2000). Measuring information transfer. *Physical Review Letters*, 85(2), 461–464.
- 431 Simony, E., Honey, C. J., Chen, J., & Hasson, U. (2016). Uncovering stimulus-locked network dynamics  
432 during narrative comprehension. *Nature Communications*, 7(12141), 1–13.
- 433 Spearman, C. (1904). General intelligence, objectively determined and measured. *American Journal of  
434 Psychology*, 15, 201–292.
- 435 Sporns, O., & Honey, C. J. (2006). Small worlds inside big brains. *Proceedings of the National Academy of  
436 Science USA*, 103(51), 19219–19220.
- 437 Tipping, M. E., & Bishop, C. M. (1999). Probabilistic principal component analysis. *Journal of Royal Statistical  
438 Society, Series B*, 61(3), 611–622.
- 439 Tong, F., & Pratte, M. S. (2012). Decoding patterns of human brain activity. *Annual Review of Psychology*, 63,  
440 483–509.

- <sup>441</sup> Turk-Browne, N. B. (2013). Functional interactions as big data in the human brain. *Science*, 342, 580–584.
- <sup>442</sup> van der Maaten, L. J. P., & Hinton, G. E. (2008). Visualizing high-dimensional data using t-SNE. *Journal of Machine Learning Research*, 9, 2579-2605.
- <sup>443</sup>
- <sup>444</sup> Zar, J. H. (2010). *Biostatistical analysis*. Prentice-Hall/Pearson.